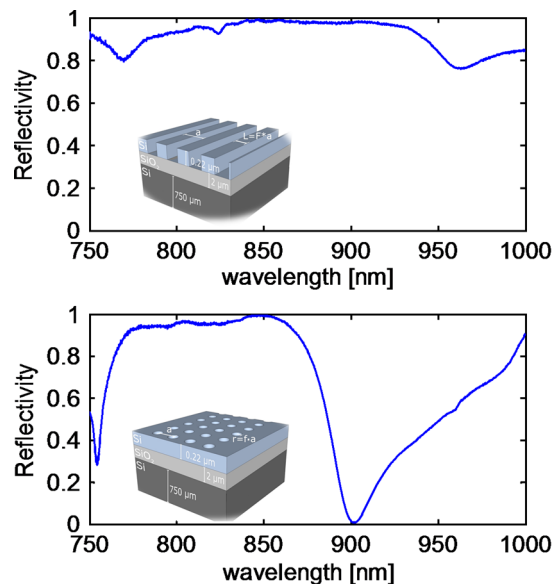# Broadband Mirrors in the Near-Infrared Based on Subwavelength Gratings in SOI

Volume 2, Number 5, October 2010

Armando Ricciardi
Stefania Campopiano
Andrea Cusano
Thomas F. Krauss
Liam O'Faolain

Broadband Mirrors in the Near-Infrared Based on Subwavelength Gratings in SOI

Armando Ricciardi,[1,2] **Stefania Campopiano,**[2] **Andrea Cusano,**[3]
Thomas F. Krauss,[1] **and Liam O'Faolain**[1]

[1]School of Physics and Astronomy, University of St. Andrews, St Andrews, KY16 9SS, U.K.
[2]Department for Technologies, University of Naples "Parthenope," 80143 Naples, Italy
[3]Optoelectronic Division, Department of Engineering, University of Sannio, 82100 Benevento, Italy

Abstract: We describe the design, fabrication, and characterization of high-reflectivity broadband mirrors operating in the near-infrared (700–1000 nm) wavelength range. The mirrors consist of 1-D and 2-D subwavelength resonant gratings (SWGs) fabricated on a silicon-on-insulator (SOI) wafer. A very good agreement between numerical and experimental results is obtained. The mirror response can be tailored by adjusting the geometrical parameters of the gratings, with the grating period as the main parameter. The optimized mirrors reflect strongly ($> 95\%$) over a fractional optical bandwidth $\Delta\lambda/\lambda$ of about 12% and 7.5% for 1-D and 2-D gratings, respectively. The important and somewhat surprising feature of these gratings is that high reflectivities have been achieved, despite the fact that silicon exhibits significant absorption in this wavelength range.

Index Terms: Mirrors, gratings, photonic crystals.

1. Introduction

Near-infrared (NIR) radiation is promising for many applications, such as free-space optical interconnects, but especially in biomedical photonics because of the relatively low absorption ("therapeutic window") of tissue in this wavelength range. As a consequence, it is possible to achieve a penetration depth of up to several centimeters, which is significant for uses ranging from clinical diagnosis to molecular biology, including optical coherence tomography (OCT) imaging [1]. Designing optical devices based on high refractive index contrast such as Bragg mirrors in this wavelength range (typ. 700–1000 nm) is not always easy, as many semiconductor-based structures, especially silicon, are limited by material absorption losses. For example, Distributed Bragg Reflectors (DBRs) require tens of layers in order to achieve the desired high reflectivities. This is both costly and makes such mirrors difficult to integrate. Alternatively, metallic mirrors may also be used, but they exhibit inferior reflectivity and their flat wavelength response precludes bandpass filtering. The subwavelength resonant gratings (SWGs) discussed here, in contrast, consist of a single layer only and can achieve broadband reflectivities larger than 99% [3]. SWGs are typically 1-D gratings, usually with high refractive index contrast, and are used in normal incidence. Two-dimensional versions have also been demonstrated [4].

SWG operation is based on a resonant phenomenon that is also known as the guided-mode resonance effect. This effect has been studied extensively in the literature [5]–[7]. The resonances arise when a normally incident wave is coupled with the *leaky* waveguide modes supported by the slab. In practice, the grating acts as a diffractive element that facilitates coupling from out-of-plane
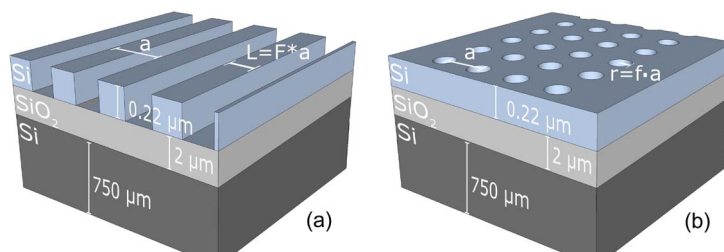
Fig. 1. Diagram of a 1-D (a) and a 2-D (b) SWG on an SOI wafer.

to in-plane waves, as well as a waveguide grating reflector for these in-plane waves. Upon reflection, the process is reversed and the waves re-emerge in reflection [8]. The overall spectral characteristics are given by the interference between the directly transmitted wave (which experiences the Fabry–Perot effect due to the light interaction with an effectively homogeneous dielectric multilayer structure) and the waves generated by the excited equivalent waveguide *leaky* modes [5]. By appropriately designing the physical and geometrical parameters, it is possible to determine the number of modes involved in the coupling process and to consequently engineer the resonant leaky-mode spectral band [9].

Owing to the versatile properties offered by resonant SWGs and their simple structure, applications as high-Q laser cavities, narrow transmission/reflection filters and sensors, have already been proposed and demonstrated [10]–[12]. One drawback of 1-D SWG mirrors, especially in comparison with DBR mirrors, is their dependence on polarization. This can be addressed by using 2-D SWGs that, in principle, are suitable for polarization independent operation. Moreover, the connected nature of 2-D SWGs makes them mechanically more robust, which is important, for example, for their use as scanning mirrors. So far, a high-reflectivity broadband mirror based on 2-D SWG has only been demonstrated experimentally in the IR wavelength range (1345–1490 nm) [13].

Previous work on 1-D SWGs in the NIR has only been based on Gallium Aluminum Arsenide (GaAs/AlGaAs) [10]. The GaAs/AlGaAs system has the advantage of low absorption loss at shorter wavelength due to the higher bandgap compared with silicon, but the high material cost makes it unattractive for high-volume, low-cost applications. Additionally, GaAs is not a suitable material for the fabrication of advanced micromechanical components. Silicon-on-insulator (SOI) is much more attractive, with very mature microelectromechanical systems technology that allows the tailoring of mechanical and electrical properties in a very uniform manner and with readily available and cost effective mass manufacture facilities. However, in the NIR, silicon-based devices are strongly affected by material absorption losses that may be prohibitive. Here, we experimentally demonstrate that it is also possible to obtain high-reflectivity mirrors in the NIR range by fabricating SWGs on a SOI wafer (see Fig. 1), despite the non-negligible absorption. Moreover, we perform a direct comparison between 1-D and 2-D SWGs and show that 1-D structures are better in terms of fabrication tolerances and high-reflectivity bandwidth.

2. Design, Fabrication, and Testing

We chose an SOI wafer with a 220 nm top silicon layer with 2 μm of buried oxide for its compatibility with CMOS foundries for Photonics (e.g., www.ePIXfab.com). The thickness of the device is also conveniently close to the optimum for the target wavelength range, and the buried oxide provides the required low index cladding.

With reference to Fig. 1, the only two parameters that we can optimize in our SWG design are the period a and the duty cycle F (fill-factor in the 2-D case), since film thickness and refractive index contrast are fixed. The duty cycle is defined as the ratio between the high refractive index layer width and the period; in the 2-D case, the fill-factor describes the relative area of the high index material and, for circular holes, is defined as $F = 1 - \pi f^2$, where f is the radius-to-pitch ratio. In order to calculate the reflectivity of the 1-D gratings, we have used the rigorous coupled-wave analysis (RCWA) [14], which is an effective and rigorous method for solving diffraction problems.
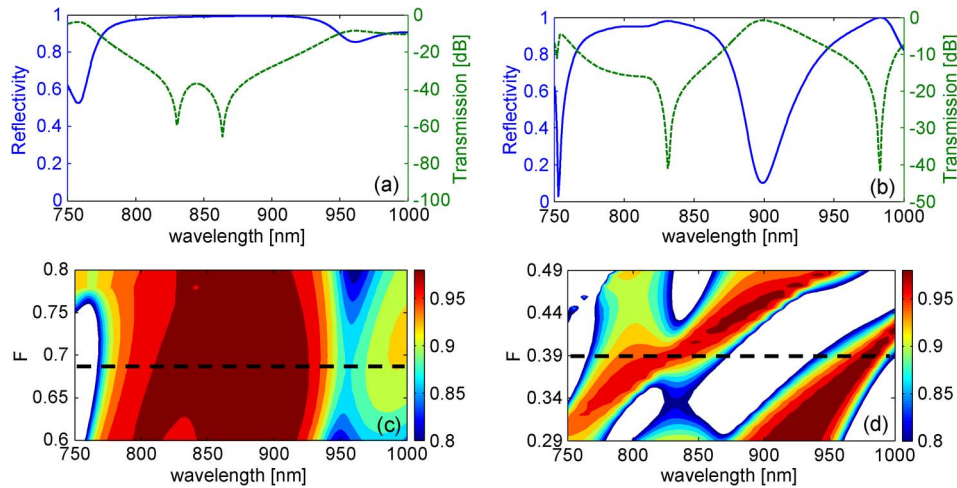
Fig. 2. Simulated reflectivity (blue continuous lines) and transmission in logarithmic scale (dashed green lines) for 1-D (a) and 2-D (b) SWG. The lattice constants and fill factors were chosen for maximum reflectivity and bandwidth in the near-IR, i.e., $a = 340$ nm and $F = 0.68$ in (a) and $a = 500$ nm and $F = 0.39$ in (b). Contour plots of reflectivity versus the duty cycle (c)/fill factor (d). The operating points chosen in (a) and (b) are indicated by a dashed line.

The number of retained diffractive orders in the calculation was chosen to be 21 in order to obtain a good convergence and stability of the results. For 2-D structures, we have used the finite-element commercial software package COMSOL Multiphysics (RF module) [15]. The computational domain is composed of one quarter of the supercell (in view of the symmetry) sandwiched between a 1.5 μm air layer (at the illuminated side) and a 2 μm layer of silica on top of a 1.5 μm layer of bulk silicon (at the other side, cf. Fig. 1). The computational domain is transversely terminated with two horizontal perfectly electric-conducting and two vertical perfectly magnetic-conducting walls to simulate a normally incident plane-wave illumination with vertically polarized electric field and is discretized using a hexahedral mesh of at least 15 lines per wavelength. Also, in this case, convergence checks and stability analysis with respect to variations in the thicknesses of the air and bulk silicon layers were successfully performed. Both the dispersion and absorption of silicon have been taken into account in our simulations.

Concerning the 1-D SWG design, we have focused the attention on transverse magnetic (TM) modes (electric field oriented orthogonally to the grating lines) because TM modes generate the broadband reflection effect at a shorter wavelength range for the same grating parameters, due to their lower effective index [16]. Moreover, the excitation of TM modes generates a larger bandwidth window for high reflectivity, as it is generally simpler to create an interaction with two or three of these modes [17].

From our calculations, we find that the largest bandwidth for high reflectivity (larger than 99% in the range 838–918 nm; see Fig. 2) is obtained for values of a and F of 340 nm and 0.68, respectively. For the 2-D SWGs, we chose values of a and F of 500 nm and 0.39, respectively, yielding reflectivities above 95% in the range 798–850 nm (larger than 90% in the range 775–865 nm).

Fig. 2(a) and (b) displays the calculated reflectivity on a linear scale and the transmission on a logarithmic scale. The log-plot shows two clear transmission dips inside the SWG reflection window, indicating that the broadband reflection is due to the interaction of waves excited by two TM leaky modes. On the other hand, the transmission dips for the case of 2-D SWGs are quite separated, allowing a gap to form between these modes. This gap creates the dip in the reflection spectrum around 900 nm, thus reducing the high-reflectivity bandwidth relative to SWGs. Moreover, the bandwidth of the resonances for the 2-D case is significantly narrower than for the 1-D, due to the higher value of the "average" refractive index that gives a longer photon lifetime inside the slab.

Fig. 2(c) and (d) displays contour plots of reflectivity versus duty cycle (c) and reflectivity versus fill factor (d). The fill factor is the most critical parameter in the fabrication process since small
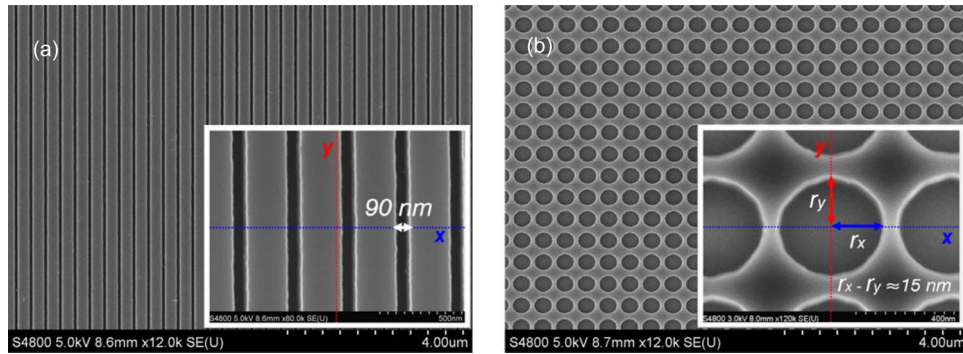
Fig. 3. SEM images of the fabricated 1-D (a) and 2-D (b) devices. The air lines width in the inset of (a) is about 90 nm, corresponding to a value of $F = 0.74$. The inset of (b) shows the ellipticity of the patterned holes. The difference between the hole radii along the two perpendicular directions is of about 15 nm ($r_x \approx 220$ nm and $r_y \approx 205$ nm).

variations during the lithographic exposure, resist development, or dry etching processes can perturb the final geometries significantly. It is evident from Fig. 2(d) that in the case of 2-D SWG, the high-reflectivity window is very sensitive to the value of the fill factor/hole radius. For example, a variation between $F = 0.29$ to 0.49, which corresponds to a difference in radius of about 36 nm, causes a dramatic difference in the reflection spectrum. By comparison, the reflectivity of 1-D SWGs is much less sensitive to variations than 2-D structures, and therefore, 1-D structures are more tolerant to fabrication errors. This is a consequence of the different bandwidths of 1-D and 2-D SWGs; a change in the duty cycle/filling factor causes a variation of both the center wavelength and the bandwidth, but evidently, the broader the resonance the less evident the change.

The patterns were defined in ZEP-520A electron beam resist using a ZEISS GEMINI 1530/RAITH ELPHY PLUS electron beam writer. The pattern was then transferred into the top silicon layer using low power (20 W), low DC bias (205 V), reactive ion etching (RIE) with a combination of SF6 and CHF3 gas (50:50 mix). The remaining resist was then removed with dimethlyacetamide. This process is based on that of [18] and has been shown to provide very high quality devices with smooth vertical sidewalls.

Fig. 3 shows scanning electron microscope (SEM) images of the fabricated structures. The fabrication process is relatively simple and requires no membraning step as in [18], since a symmetric cladding is not required for the successful operation of SWGs. To provide an even more robust device, an oxide cladding may be employed, as in [19].

The fabricated samples were characterized in reflection with a broadband white light source (KOHERAS Super-K Compact) sent through a polarizer and a beamsplitter. Light reflected from the grating returns through the beam splitter and is sent to the OSA for spectral analysis. The area of the gratings was 500 μm × 500 μm. The measured spectral intensity is normalized by dividing by the reflection spectrum of a gold coated mirror with a reflectivity larger than 97.5% ($> 98\%$ for $\lambda > 800$ nm) over the entire analyzed wavelength range; therefore, the reported values can be considered absolute within the measurement accuracy. The gold mirror spectrum was measured using a Perkin Elmer Lambda 950 UV/VIS Spectrophotometer.

The measured reflection spectra (continuous lines) are plotted in Fig. 4 and compared with numerical data (dashed black lines) for the 1-D [see Fig. 4(a) and (c)] and the 2-D [see Fig. 4(b) and (d)] SWG. The blue and red lines indicate the two different polarizations of the incident wave. In particular, with respect to the insets of Fig. 3, the blue and red lines refer to an electric field polarized along x and y, respectively. As expected, the SWG behavior is different for the two polarizations, being optimized to reflect strongly only TM. On the contrary, the 2-D SWG should, in principle, be polarization independent; as shown in Fig. 4(b) and (d), this is clearly not the case, and the broadband reflectivity has been obtained only for one polarization (POL I). The reason for this is the narrowness of the target operating window in Fig. 2(d). Consequently, the slight, i.e., $\Delta r \approx 15$ nm, ellipticity of the patterned holes, as shown in the inset of Fig. 3(b), is very significant. We believe
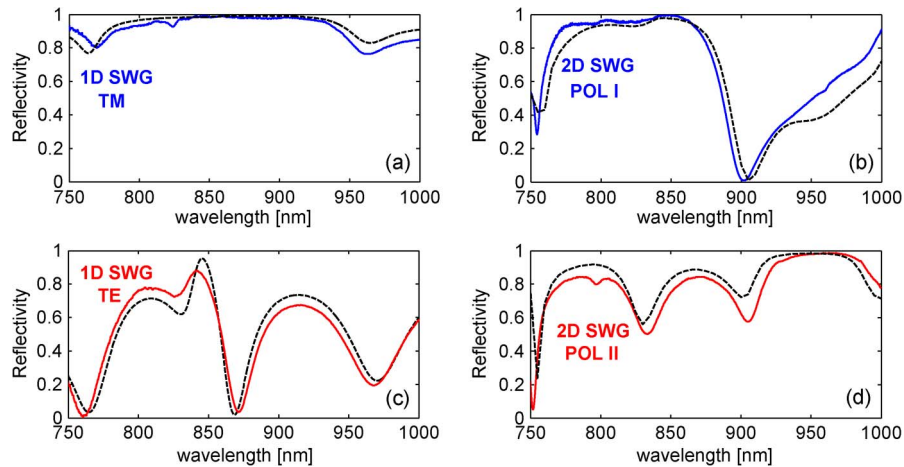
Fig. 4. Experimental (continuous lines) and numerical (dashed black lines) reflection spectra for the 1-D SWG (a) and (c) and the 2-D SWG (b) and (d). The blue (electric field directed along x—see Fig. 3) and red lines (electric field directed along y) indicate the two different polarization of the incident wave. The parameters used to calculate the numerical spectra for 1-D SWG are $a = 340$ and $F = 0.74$. For the 2-D case, we have simulated the lattice with $a = 500$ nm and with an elliptical hole of radii $r_x = 222$ nm and $r_y = 208$ nm corresponding to a ratio of 93.7%.
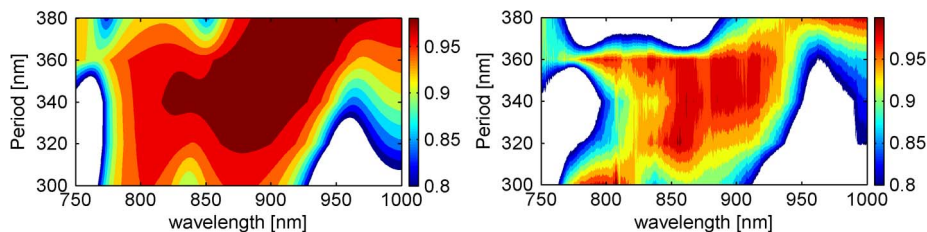

Fig. 5. Numerical (a) and experimental (b) 1-D SWG spectra contour plot. The experimental data refer to SWGs with a period of 300 nm–380 nm in 20 nm steps, the intermediate points having been interpolated. The color scheme divides the 80%–100% reflectivity range into 10 steps of 2% each.

that this is a result of a slight astigmatism of the electron beam. In practice, the resulting structure has two different values of F along the two symmetry axes of the structure. For POL I the fill-factor is very close to the optimized one (i.e., $F = 0.39$) while for POL II $F \approx 0.47$. In fact, the sensitivity of these structures to ellipticity could be used as a probe for the accuracy of the e-beam exposure.

For TM polarization, the measured spectrum of the 1-D SWG has a reflectivity larger than 90% over a wavelength range of 160 nm (782–942 nm), which corresponds to a fractional optical bandwidth $\Delta\lambda/\lambda$ of about 18.5%. The reflectivity is even higher ($> 95\%$) in the wavelength range 826 nm–933 nm ($\Delta\lambda/\lambda \sim 12\%$). By comparison, the 2-D SWG reflectivity is larger than 90% over a 100 nm band centered at 820 ($\Delta\lambda/\lambda \sim 12\%$) and $> 95\%$ in the range 800–864 nm ($\Delta\lambda/\lambda \sim 7.5\%$).

Despite of the use of a strongly absorptive material at NIR wavelengths, very high values of reflectivity have thus been obtained. This can be explained by taking into account that the modes excited in the SWG have an overlap of around 50% with the absorbing silicon material and that the penetration depth of these modes into the grating is only a few micrometers due to the strong index contrast [20]; combined with the absorption length of bulk silicon at $\lambda = 800$ nm of around 10 μm, it becomes clear that only a few percent of light are lost to absorption, even at such relatively short wavelengths as $\lambda = 800$ nm.

To evaluate the option of tuning the wavelength response of the grating via the lattice constant, we characterized five different SWGs fabricated with lattice constants of 300, 320, 340, 360, and 380 nm and a fixed duty cycle. In Fig. 5, both numerical (a) and experimental (b) contour plots are shown, demonstrating a good agreement. The main discrepancy is the fact that the reflectivity

values are slightly lower for the experimental plot, which is not surprising given the presence of fabrication imperfections. Overall, it is evident that by increasing the grating period, the high-reflectivity band shifts toward higher wavelengths, giving a degree of control that is absent with thin metal films and DBR mirrors.

3. Conclusion

We have presented the first experimental demonstration of 1-D and 2-D SWG mirrors fabricated on SOI wafers working in the NIR. The mirrors are broadband (typ. $\Delta\lambda > 100$ nm) and exhibit high reflectivity in the 700–1000 nm wavelength range. Our 1-D SWG mirrors are tolerant to fabrication errors and can be tuned by simply modifying their geometrical parameters, e.g., the pitch and fill-factor. Measured reflectivities larger than 95% have been obtained, demonstrating that silicon absorption is not a strong limitation for this particular application.

We have also studied 2-D SWG mirrors and have shown that they have lower reflectivity and are less fabrication tolerant. We note that the expected polarization independence is difficult to obtain because the grating response is very sensitive to the shape of the holes; any ellipticity, even as small as a few nanometers, is sufficient to induce significant changes.

Overall, we have demonstrated that SWGs are powerful building blocks for devices operating in the technologically important NIR range, with significant advantages over competing high-reflectivity mirrors such as DBRs and metallic coatings.

Acknowledgment

References

[1] R. Weissleder and V. Ntziachristos, "Shedding light onto live molecular targets," *Nat. Med.*, vol. 9, no. 1, pp. 123–128, Jan. 2003.

[2] J. S. Milne, J. M. Dell, A. J. Keating, and L. Faraone, "Widely tunable MEMS-based Fabry–Perot filter," *J. Microelectromech. Syst.*, vol. 18, no. 4, pp. 905–913, Aug. 2009.

[3] C. F. R. Mateus, M. C. Y. Huang, D. Yunfei, A. R. Neureuther, and C. J. Chang-Hasnain, "Ultrabroadband mirror using low-index cladded subwavelength grating," *IEEE Photon. Technol. Lett.*, vol. 16, no. 2, pp. 518–520, Feb. 2004.

[4] B.-H. Cheong, O. N. Prudnikov, E. Cho, H.-S. Kim, J. Yu, Y.-S. Cho, H.-Y. Choi, and S. T. Shin, "High angular tolerant color filter using subwavelength grating," *Appl. Phys. Lett.*, vol. 94, no. 21, p. 213 104, May 2009.

[5] S. S. Wang and R. Magnusson, "Theory and applications of guided-mode resonance filters," *Appl. Opt.*, vol. 32, no. 14, pp. 2606–2613, May 1993.

[6] R. Magnusson and M. Shokooh-Saremi, "Physical basis for wideband resonant reflectors," *Opt. Express*, vol. 16, no. 5, pp. 3456–3462, Mar. 2008.

[7] S. H. Fan and J. D. Joannopoulos, "Analysis of guided resonances in photonic crystal slabs," *Phys. Rev. B, Condens. Matter*, vol. 65, no. 23, p. 235 112, Jun. 2002.

[8] D. Rosenblatt, A. Sharon, and A. A. Friesem, "Resonant grating waveguide structures," *IEEE J. Quantum Electron.*, vol. 33, no. 11, pp. 2038–2059, Nov. 1997.

[9] Y. Ding and R. Magnusson, "Resonant leaky-mode spectral-band engineering and device applications," *Opt. Express*, vol. 12, no. 23, pp. 5661–5674, Nov. 2004.

[10] M. C. Y. Huang, Y. Zhou, and C. J. Chang-Hasnain, "A surface-emitting laser incorporating a high-index-contrast subwavelength grating," *Nature Photon.*, vol. 1, no. 2, pp. 119–122, Feb. 2007.

[11] P. S. Priambodo, T. A. Maldonado, and R. Magnusson, "Fabrication of characterization of high-quality waveguide-mode resonant optical filters," *Appl. Phys. Lett.*, vol. 83, no. 16, pp. 3248–3250, Oct. 2003.

[12] C. F. R. Mateus, M. C. Y. Huang, P. Li, B. T. Cunningham, and C. J. Chang-Hasnain, "Compact label-free biosensor using VCSEL-based measurements system," *IEEE Photon. Technol. Lett.*, vol. 16, no. 7, pp. 1712–1714, Jul. 2004.

[13] I. W. Jung, S. Kim, and O. Solgaard, "High-reflectivity broadband photonic crystal mirror MEMS scanner with low dependence on incident angle and polarization," *J. Microelectromech. Syst.*, vol. 18, no. 4, pp. 924–932, Aug. 2009.

[14] M. G. Moharam, D. A. Pommet, E. B. Grann, and T. K. Gaylord, "Stable implementation of the rigorous coupled-wave analysis for surface-relief gratings: Enhanced transmittance matrix approach," *J. Opt. Soc. Amer. A, Opt. Image Sci.*, vol. 12, no. 5, pp. 1077–1086, May 1995.

[15] [Online]. Available: http://www.comsol.com/

[16] C. Gu and P. Yeh, "Form birefringence dispersion in periodic layered media," *Opt. Lett.*, vol. 21, no. 7, pp. 504–506, Apr. 1996.

[17] M. Shokooh-Saremi and R. Magnusson, "Wideband leaky-mode resonance reflectors: Influence of grating profile and sublayers," *Opt. Express*, vol. 16, no. 22, pp. 18 249–18 263, Oct. 2008.

[18] L. O'Faolain, X. Yuan, D. Mcintyre, S. Thoms, H. Chong, R. M. De la Rue, and T. F. Krauss, "Low-loss propagation in photonic crystal waveguides," *Electron. Lett.*, vol. 42, no. 25, pp. 1454–1455, Dec. 2006.

[19] T. P. White, L. O'Faolain, J. Li, L. C. Andreani, and T. F. Krauss, "Silica-embedded silicon photonic crystal waveguides," *Opt. Express*, vol. 16, no. 21, pp. 17 076–17 081, Oct. 2008.

[20] J. M. Bendickson, E. N. Glytsis, T. K. Gaylord, and D. L. Brundrett, "Guided-mode resonant subwavelength gratings: Effects of finite beams and finite gratings," *J. Opt. Soc. Amer. A, Opt. Image Sci.*, vol. 18, no. 8, pp. 1912–1928, Aug. 2001.